www.gondwanags.org.in

Original Article

ISSN : 2455-1953

JGSR

Journal of Geosciences Research

Vol. 7, No.2, July, 2022, pp. 186-192

Geochemistry and Phase Equilibrium Modelling of Garnet-Biotite Gneiss from Mauranipur, Bundelkhand Craton, Northern India: Implication for Tectonic Setting and Metamorphism

Pratigya Pathak*, Shyam Bihari Dwivedi and Ravi Ranjan Kumar

Department of Civil Engineering, Indian Institute of Technology (BHU), Varanasi-221005(UP), India
*(*Corresponding author, E-mail: pratigyapathak.rs.civ17@itbhu.ac.in)*

Abstract

The Mauranipur region is situated along the central part of the Bundelkhand Craton (BuC) in the northern Indian shield, which consists of garnet-biotite gneisses with various deformational structures in the form of folding, faulting, augen and tail structures. These deformation structures are tectonic imprints that reveal the tectonic nature of the garnet-biotite gneisses. The groundmass of Grt-Bt gneisses is characterized by presence of garnet, biotite, plagioclase, K-feldspar, quartz, and ilmenite. The phase equilibrium modelling and geochemical attributes depict the tectonic activity and metamorphic evolution of the studied rocks. The *P-T* pseudosection has been calculated in the NCKFMASHT system, which revealed that the peak mineral assemblage stabilized in the *P-T* range of 6.35–6.75 kbar and 755–780ºC, and it further goes to retrograde metamorphism under *P-T* condition ranging from 4.80–5.28 kbar and 718–735ºC. These gneisses represent a calc-alkaline to high-K calc-alkaline series of protolithic origin. The negative anomaly of Nb and Ti for all samples indicates that a subduction tectonic setting has occurred in the BuC. The $(La/Lu)_N$ ratio and differences in the trace elements indicate heterogeneous sources and large variation in the degree of partial melting. The Y *vs* Nb and (Y+Nb) vs Rb tectonic discrimination diagrams indicate that the Grt-Bt gneisses have an affinity towards the volcanic arc granite and developed during subduction setting. The geochemical interpretation provides significant evidence that protoliths of Grt-Bt gneisses were further metamorphosed by the continent-continent collision.

Keywords: Garnet-biotite gneiss, Pseudosection, *P-T* condition, Geochemistry, Bundelkhand

Introduction

Geologists have always been curious to know about the compositional character of the Archean continental crust (Barik *et al*., 2017). The most challenging problem is to understand the nature of the geodynamic and petrogenetic processes responsible for the origin of Archean continental crust (Zhai, 2014). The ubiquitous association of tonalite-trondhjemite-granodiorite gneisses (TTG), amphibolites, metavolcanic and metasedimentary rocks with greenstone rocks is a common feature of the Archean cratons (Naqvi, 2005). The Archean craton and orogenic belts are dominated by gneisses, migmatites and granulites, which are formed during exhumation processes. Therefore, these rocks preserve valuable sources of information and may help to decipher the petrogenesis and metamorphic evolution of the Archean continental crust.

The Bundelkhand Craton (BuC) is an important unit in the northern portion of the Indian Peninsula (Gokarn *et al.,* 2013). The central part of BuC consists predominantly of high-grade supracrustal rocks, composed of garnet–sillimanite–cordierite gneisses and garnet-biotite gneisses with a metamorphic *P-T* condition of 5.1–5.4 kbar/640–730°C (Singh and Dwivedi, 2009). But, the metamorphic evolution and tectonic behavior of these high-grade rocks are yet to be studied in detail. Therefore, it is reliable to conduct detailed geochemical studies to understand Grt-Bt gneisses. This paper focuses on studying major, trace and rare earth elements of various representative samples of Grt-Bt gneisses from the Mauranipur area of the BuC. Geochemical studies reveal the protolithic nature and tectonic setting of Grt-Bt gneisses, and further metamorphic changes have been understood by *P-T* pseudosection modelling.

(Received : 07 July 2021 ; Revised Form Accepted : 20 January 2022)

https://doi.org/10.56153/g19088-021-0048-2

Geological Setting

The Indian peninsula consists mainly of two vital Archean crustal blocks: a northern (Bundelkhand and Aravali) and a southern (Dharwar, Singhbhum and Bastar) crustal block (Kaur *et al*., 2014). These two Archean blocks amalgamated along the E-W trending Central Indian Tectonic Zone (CITZ) during the Paleo-Mesoproterozoic subduction–accretion–collision (Bhowmik *et al*., 2012). The northern crustal block can be divided into two cratonic blocks, separated by the Great Boundary Fault (Mohan *et al*., 2012). The western block is the Aravali Craton, while the eastern block is

the BuC (Fig.1a). The BuC is semi-circular in configuration, with an area of about 26,000 km^2 (Singh *et al*., 2021). The Son-Narmada fault binds the BuC in the south, and the Yamuna fault in the north separates it from the Himalayas (Singh *et al.,* 2007). Marginal basins such as Gwalior, Sonrai and Bijawar bind the BuC from north-west, south and south-east, respectively (Kaur *et al*., 2014; Saha *et al*., 2011). The Vindhyan Supergroup is present overlying the marginal basins and binds the BuC on three sides, whereas the southwest portion is hidden under the Deccan basalts (Fig.1b). The BuC is dominated by TTGs and granitoids of 3.5–2.6 Ga age, and also includes various enclaves of high-grade gneisses, quartzites, meta-ultrabasic rocks, BIFs and calc-silicates (Singh *et al*., 2021). Apart from these, Sharma and Rahman (2000) has recognized three lithological units. The first unit is highly deformed TTGs and greenstones of the Archean age (3.59–2.6 Ga) (Kaur *et al.,* 2021), the second unit is granitoid that exists as a pluton of the Proterozoic age (2.6–2.1 Ga) (Joshi *et al.,* 2017). The last unit has occurred in the form of mafic dyke swarms (dolerites and gabbroic rocks) with three episodic evidences of 1.98, 1.8 and 1.0 Ga (Pradhan *et al.,* 2012). The Paleoproterozoic sedimentary rocks of the Gwalior and Bijawar basins are deposited over the TTGs complex and metavolcanic, migmatites and amphibolites (Pati, 2020; Singh *et al.,* 2019).

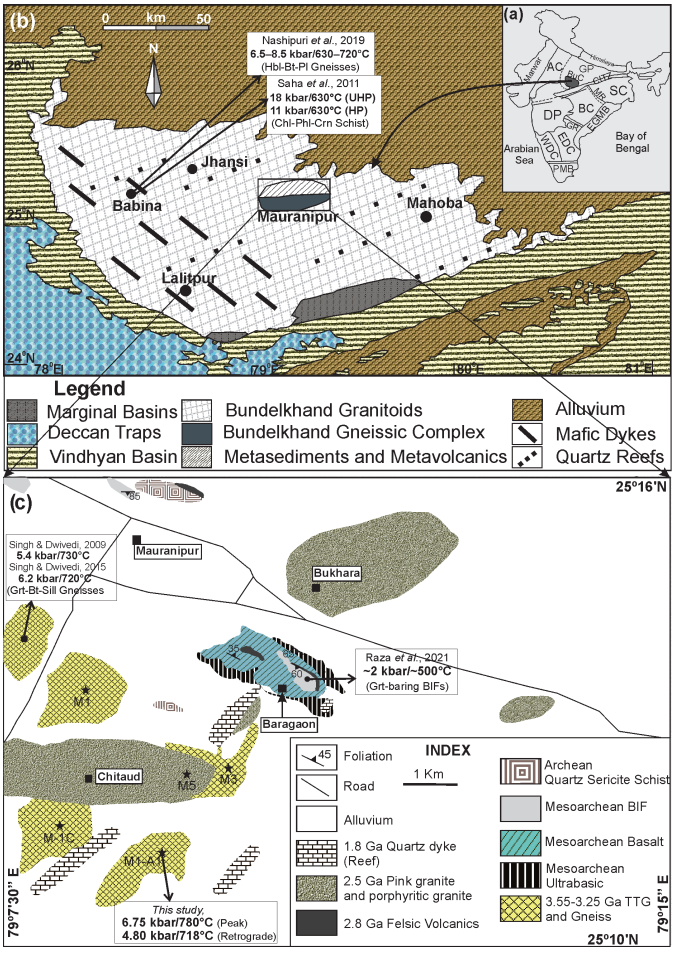

Fig. 1. (a) The map of India representing different cratonic blocks, abbreviations; AC: Aravali Craton, BC: Bastar Craton, BuC:, Bundelkhand Craton, CITZ: Central Indian Tectonic Zone, DP: Deccan Plateau, EDC: Eastern Dharwar Craton, EGMB: Eastern Ghat Mobile Belt, GP: Gangetic Plain, GR: Godavari Rift, MR: Mahanadi Rift, PMB: Pandyan Mobile Belt, SC: Singhbhum Craton, WDC: Western Dharwar Craton, (*after*, Singh and Dwivedi, 2015) (b) A simplified geological map of the Archean BuC (*after* Singh and Dwivedi, 2015). (c) Geological map of Mauranipur area (*after* Singh *et al.,* 2018).

The BuC is classified in two belts, the first is the Central Bundelkhand Greenstone Belt (CBGB), which runs from Babina to Mahoba via Mauranipur, and the second is known as Southern Bundelkhand Greenstone Belt, which passes from Madaura to Girar (Singh and Slabunov, 2013). The CBGB is further classified into two greenstone belts: Mauranipur and Babina greenstone belts with E-W trending, including ultramafic-mafic and felsic volcanics as well as metasedimentary units (BIFs) of Paleoarchean age, and are medium to low-grade metamorphosed (Nasipuri *et al*., 2019). The studied samples have been collected from the Sarprar river section near the Kuraicha and Mauranipur area (Fig.1c), within the Mauranipur-Babina greenstone belt. The area of investigation is located between latitude 25°10' N to 25°16' N and longitude 79°15' E to 79°30' E. The study area includes TTGs, gneisses, granitoids, mafic-ultramafic rocks, basalts, BIFs, quartz-sericite schist, felsic volcanics, pink granites and quartz reefs.

Analytical Techniques

EPMA Analysis

The mineral chemistry was studied using an electron probe microanalyzer (EPMA) CAMECA SX Five instrument at DST–SERB National Facility, Department of Geology (BHU), Varanasi. Natural mineral standards (Pandey *et al.*, 2017) were acquired at 15 kV of acceleration voltage and 10 nA beam current.

Whole Rock Analysis

Analyses of the rock samples for major, trace and REE was done at Birbal Sahni Institute of Palaeosciences, Lucknow. Samples were prepared by the pressed powder method using boric acid as a binder (boric acid: sample ratio, 2:3). Major oxides were analyzed by X-ray fluorescence (XRF) using wavelength dispersive (WD-XRF AXIOS MAX) machine with power: 4KW, 60kV-160 mA analytical, on pressed powder pellet machine used 'kameyo' at pressure 15-20 ton, with 4mm pallet thickness. The USGS Rock Standard used were BCR-2, BHVO-1, RGM-2, and GSP-2.

Trace and Rare earth elements (REEs) were analyzed by ICP-MS (Make: Agilent, Model: ICP-MS 7700x). The USGS Rock Standards used were BCR-2, BHVO-1, RGM-2, and GSP-2. All solutions were prepared using ultrapure water (18.2 MX). All the samples were digested by taking 30 mg (300 mesh) sediment powder using supra pure acid (HF, $HClO_4$, HNO_3) (Xiong *et al.,* 2012). The accuracy of measurement of both the instruments is within 2-10% and precesion is <2%.

Petrography and Mineral Chemistry

Petrography

The Grt-Bt gneisses exist as enclaves within the TTG gneisses throughout the study area. They show typical gneissose banding composed of melanocratic and leucocratic mineral-rich layers and are medium to coarse grained. Various structural features have been observed in Grt-Bt gneisses, such as folding (Fig.2a), faulting (Fig.2b), and augen-tail structure (Fig.2c). Grt-Bt gneisses

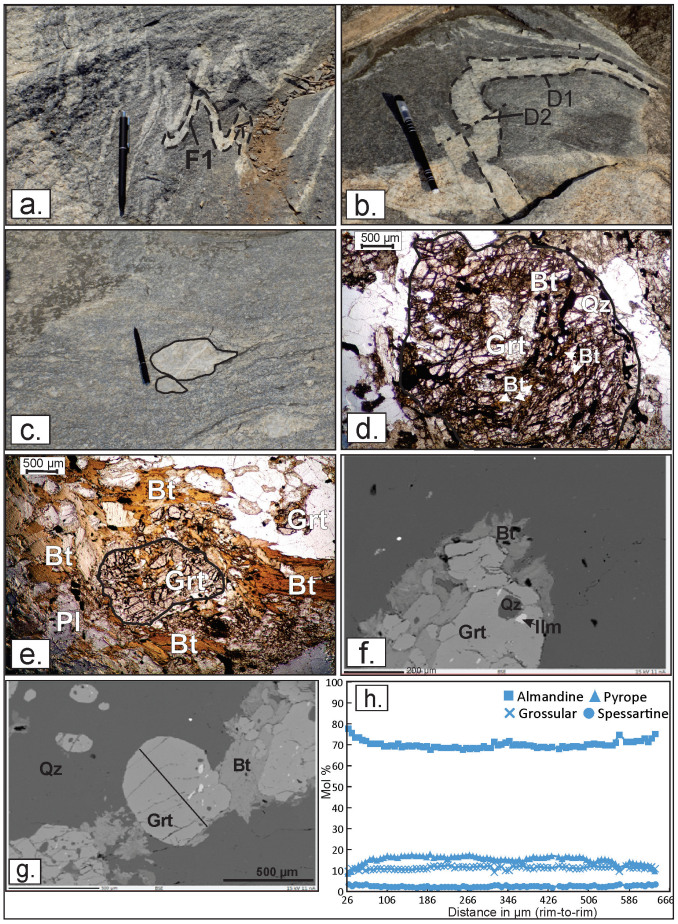

Fig. 2. Field photographs of Grt-Bt gneisses of the BuC (a) folding, (b) faulting and, (c) augen and tail structure. Photomicrographs are showing (d) quartz and biotite included within garnet porphyroblast, (e) garnet surrounded by biotite and quartz. BSE image showing (f) quartz and ilmenite present in garnet, (g) garnet porphyroblast, (h) X_{Alm}, X_{Py}, X_{Grs} and X_{Sps} variation along the garnet porphyroblast from rim to rim. Abbreviations are taken from Whitney and Evans (2010).

Table 1: EPMA and structural formula of garnet from the garnet-biotite gneiss (Sample M1-A1).

Domain	27	28	31	58	52	60
SiO_2	37.057	36.932	37.137	36.563	36.857	37.540
TiO_2	0.042	0.054	0.049	0.135	0.090	0.084
Al_2O_3	21.156	20.933	20.814	20.471	20.565	20.012
FeO	33.207	33.481	33.993	30.705	31.167	30.411
MnO	1.327	1.394	1.405	1.246	1.362	1.380
MgO	3.294	3.272	2.643	3.941	3.666	3.717
CaO	4.590	3.935	4.080	6.631	6.204	6.581
Total	100.706	100.000	100.126	99.719	99.921	99.845
			12 Oxygens			
Si	2.964	2.957	2.982	2.989	2.963	2.996
Al^{IV}	0.000	0.000	0.000	0.000	0.000	0.000
∑Z	2.944	2.957	2.982	2.989	2.963	2.986
Al^{VI}	1.981	1.976	1.970	1.920	1.949	2.064
Ti	0.002	0.003	0.003	0.008	0.005	0.005
Fe^{3+}	0.132	0.104	0.060	0.252	0.114	0.000
∑Y	2.115	2.083	2.033	2.180	2.068	2.069
Fe^{2+}	2.074	2.138	2.222	1.791	1.849	1.923
Mn	0.089	0.094	0.096	0.084	0.093	0.093
Mg	0.389	0.390	0.316	0.467	0.430	0.441
Ca	0.382	0.338	0.351	0.565	0.525	0.565
∑X	2.934	2.960	2.985	2.907	2.967	2.914
Pyrope	12.69	12.73	10.38	14.78	14.13	14.14
Almandine	71.95	73.17	74.94	64.67	66.27	64.89
Grossularite	12.46	11.03	11.53	17.89	16.60	17.99
Spessartne	2.90	3.07	3.15	2.66	2.93	2.98
X_{Mg}	0.16	0.15	0.13	0.20	0.18	0.19

$X_{Mg}=Mg/(Mg+Fe^{2+})$

are mainly composed of garnet-biotite-plagioclase-K-feldspar-ilmenite-quartz. Plagioclase is lath-shaped, showing lamellar twinning along the margins of biotite and garnet. Quartz occurs as irregularly shaped crystals that exhibit undulose extinction in alliance with plagioclase, biotite and garnet. Accessory minerals include ilmenite, monazite and apatite. Garnet and biotite establish two different reaction textures, which were evolved at different stages of metamorphic conditions. The first reaction texture is defined by the garnet porphyroblast containing inclusions of biotite as well as plagioclase and quartz suggesting prograde metamorphism. This reaction texture has been observed in figure 2d, and can be depicted by the following reaction:

$$\text{Biotite} + \text{plagioclase} + \text{quartz} \rightarrow \text{garnet} + \text{K-feldspar} + \text{melt} \quad (1)$$

At some places, garnet is consumed to form biotite which shows retrograde metamorphism. This situation represents another type of reaction texture includes garnet and biotite (Fig. 2e-f), and the reaction is:

$$\text{Garnet} + \text{K-feldspar} + H_2O \rightarrow \text{biotite} + \text{quartz} \quad (2)$$

Mineral Chemistry

The mineral chemistry and line profile of garnet porphyroblast reveal that garnet are rich in Fe, Mg and Ca contents but poor in Mn content (Fig.2g-h). The garnet mainly shows solid solutions of almandine (64.67–74.94 mol%), pyrope (10.38–14.78 mol%) and grossular (11.03–17.99 mol%), with minor amounts of spessartine (2.66–3.15 mol%) (Table 1). The X_{Mg} [$Mg/(Mg+Fe^{2+})$] values of garnet suggest that two generations of garnet are present in the studied rock. Type1 garnet (porphyroblast garnet containing inclusions of biotite) has X_{Mg} values ranging from 0.13 to 0.16, and type2 garnet (garnet surrounded by biotites) has X_{Mg} values ranging from 0.18–0.20. The MgO content (2.643–3.941 wt%) in garnets is much lower than FeO content (30.411–33.993 wt%). The X_{Mg} values of biotite demarcate two-variable compositions, i.e., 0.31–0.32 (Type1) and 0.43–0.44 (Type2) (Table 2). These two different X_{Mg} values correspond to two textural types of biotites. Type1 biotite exists as inclusions within the garnet porphyroblast, and Type2 biotite rims around garnet grains. Biotite has significantly less FeO (22.56–27.38 wt%) than garnet, although higher in MgO content (6.75–9.88 wt%), and also biotite has a lower TiO_2 (1.51–1.99 wt%). The amount of Al_2O_3 ranges between 16.20–16.55 wt%, with the Al^{VI} content ranging from 0.39 to 0.53 pfu. The anorthite [An = Ca/(Ca+Na+K)] content of plagioclase shows a range of 0.45-0.62 (Table 3). The CaO content (9.65–13.14 wt%) in all the plagioclase is higher than that of Na_2O content (4.29–6.35wt%).

Phase Equilibrium Modelling

Metamorphic *P-T* conditions of the garnet-biotite-

Table 2: EPMA and structural formula of biotite, from the garnet-biotite gneiss (Sample M1-A1).

Domain	72	99	100	21	22
SiO_2	33.283	33.484	33.147	33.826	33.312
TiO_2	1.509	1.988	1.767	1.558	1.537
Al_2O_3	16.417	16.204	16.494	16.397	16.549
FeO	26.597	27.377	26.736	22.563	23.559
MnO	0.023	0	0	0	0.114
MgO	6.75	6.974	7.103	9.885	9.914
CaO	0.043	0	0.107	0.094	0.064
Na_2O	0.778	0.092	0.089	0.095	0.152
K_2O	7.31	8.923	8.169	8.988	7.903
Cl	0.097	0.087	0.076	0.025	0.013
F	0.108	0.187	0.078	0.064	0.063
Total	92.914	95.317	93.765	93.494	93.18
			22 Oxygens		
Si	5.395	5.348	5.341	5.372	5.309
Al^{IV}	2.605	2.652	2.659	2.628	2.691
∑Z	8	8	8	8	8
Al^{VI}	0.531	0.398	0.473	0.441	0.418
Ti	0.184	0.239	0.214	0.186	0.184
Fe^{2+}	3.605	3.656	3.602	2.996	3.14
Mn	0.003	0	0	0	0.015
Mg	1.631	1.661	1.706	2.34	2.356
∑X	5.954	5.953	5.996	5.963	6.113
Ca	0.007	0	0.018	0.016	0.011
Na	0.244	0.029	0.028	0.029	0.047
K	1.511	1.818	1.679	1.821	1.607
∑Y	1.763	1.846	1.725	1.866	1.665
Cl	0.027	0.024	0.021	0.007	0.003
F	0.055	0.095	0.04	0.032	0.032
X_{Mg}	0.31	0.31	0.32	0.44	0.43

X_{Mg}=Mg/(Mg+Fe^{2+})

plagioclase-K-feldspar-melt-ilmenite-quartz stable mineral assemblage have constrained using the Perple_X ver.6.9.0 software (Connolly, 2005, 2009), and end-member thermodynamic data were taken from Holland and Powell (2011). The pseudosection of the representative sample (M1-A1) has prepared in the NCKFMASHT system (Na_2O-CaO-K_2O-FeO-MgO-Al_2O_3-SiO_2-H_2O-TiO_2). The solid solution models for various minerals have been considered in this phase equilibrium modelling, such as; garnet, melt (W: White *et al*., 2014), plagioclase (HP: Holland and Powell, 2003), feldspar (feldspar: Fuhrman and Lindsley, 1988), biotite (TCC: Tajcmanová *et al.,* 2009), and ilmenite (WPH: White *et al.,* 2000). Alumino-silicates, quartz, and magnetite are treated as pure end-member phases. The measured bulk compositions of the modeled sample in mol% are: SiO_2 = 61.77, Al_2O_3 = 10.19, CaO = 2.12, FeO = 9.12, K_2O = 2.09, MgO = 8.07, Na_2O =2.11, TiO_2 =1.04 and H_2O = 3.50. MnO and P_2O_5 contents are very low; hence it is neglected in pseudosection construction, whereas P_2O_5 is used in recalculation of CaO.

Grt-Bt gneisses contain bands of leucosome as a sign of the availability of melt. Melt is an important constituent for any metamorphic rocks, so it is considered in the phase equilibria modelling. Here, the amount of H_2O is constrained with the help of T-X_{H2O} pseudosection (Fig. 3a), and it is constructed at 5.0 kbar pressure. The molar composition of H_2O is plotted along the X-axis in T-X_{H2O} pseudosection. The computed amount of H_2O varies from the anhydrous composition (X_{H2O} = 0 mol %) to excess H_2O (X_{H2O} = 8.0 mol %). The X_{H2O} (3.50 mol %) is appropriate constituent for the formation of stable mineral assemblages (Grt-Bt-Pl-Kfs-melt-Ilm-Qz).

The *P-T* pseudosection is constructed in the range of 3–8 kbar and 400–800ºC (Fig. 3b). Garnet, biotite and quartz are ubiquitous

Table 3: EPMA and structural formula of plagioclase, from the garnet-biotite gneiss (Sample M1-A1).

Domain	65	66	101	102	39
SiO_2	55.877	52.861	53.077	51.682	57.589
Al_2O_3	27.526	29.260	29.417	30.587	25.954
FeO	0.162	0.653	0.100	0.151	0.153
CaO	9.649	11.656	12.082	13.140	9.947
Na_2O	6.352	4.842	4.921	4.288	6.032
K_2O	0.086	0.112	0.057	0.132	0.054
Total	99.652	99.384	99.654	99.980	99.729
			8 Oxygens		
Si	2.524	2.413	2.413	2.351	2.592
Al	1.465	1.574	1.576	1.640	1.377
Fe^{2+}	0.006	0.025	0.004	0.006	0.006
Ca	0.467	0.570	0.588	0.640	0.480
Na	0.556	0.429	0.434	0.378	0.526
K	0.005	0.007	0.003	0.008	0.003
Total	5.024	5.017	5.018	5.022	4.984
An	45.42	56.72	57.38	62.40	47.53
Ab	54.10	42.64	42.29	36.85	52.16
Or	0.48	0.65	0.32	0.75	0.31
X_{Ca}	0.45	0.57	0.57	0.62	0.48

X_{Ca}=Ca/(Ca+Na+K)

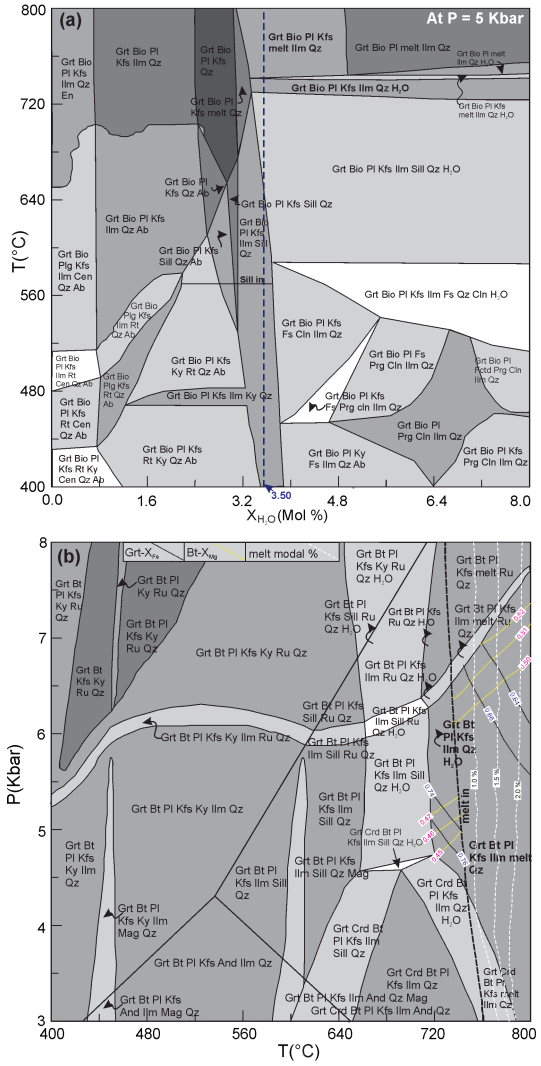

Fig. 3. (a) T–X_{H2O} pseudosection at 5.0 kbar, showing the effects of varying the molar proportions of bulk-rock H_2O, black dash line is modelled composition of H_2O (3.50 %). (b) pseudosetion (M1-A1) is calculated in NCKFMASHT system, and Isopleth lines for garnet (X_{Mg}), biotite (X_{Mg}), and melt modal %.

in the *P-T* pseudosection. The required mineral assemblage (Grt-Bt-Pl-Kfs-melt-Ilm-Qz) represented peak metamorphic assemblage and tenanted a field in the *P-T* range of 6.35–6.75 kbar and 755–780ºC. The *P-T* condition is calibrated with the help of isopleths lines of X_{Mg} garnet and X_{Mg} biotite. The calculated pseudosection is admissible for mineral assemblages observed in petrography. Instead of this, we have also observed similar mineral assemblages under lower pressure and temperature conditions. Here, the melt phase does not exist, whereas H_2O is available as a component. Therefore, we would like to say that this stable phase may evolve during the retrograde metamorphic condition. Their *P-T* condition is comparatively low, which is between 4.80–5.28 kbar and 718–735ºC.

Geochemistry

The geochemical data of the Grt-Bt gneisses are given in table 4. The Grt-Bt gneisses are compositionally variable in major oxides as; SiO_2 (57.64–77.83 wt%), Al_2O_3 (7.46–16.31 wt%), MgO (0.47–8.02 wt%), FeO (2.61–13.91 wt%), K_2O (0.99–3.13 wt%), and also contains lesser amounts of TiO_2 (0.62–1.66 wt%), CaO (1.80–3.51 wt%), Na_2O (1.03–3.26 wt%) and P_2O_5 (0.14–0.65 wt%). Samples show considerable variation in the K_2O/Na_2O ratios as 0.78–1.55, suggesting its potassium-rich character. The combined alkalis (K_2O+Na_2O) wt% is 2.03–6.11. The $Al_2O_3/(CaO+Na_2O + K_2O)$ ratio ranges between 1.00 and 2.34. The Grt-Bt gneisses are plotted on the total alkali versus silica (TAS) diagram (Fig.4a), as well as K_2O *vs* SiO_2 diagram (Fig.4b) which indicates calc-alkaline series.

The Primitive mantle normalized spider diagram of Grt-Bt gneisses reveal depletion of Mo, Ho, Tm, Ba, K, Nb, Sr, Hf, Ti, and abundance of Rb, Th, U, La, Ce, Nd and Gd (Fig.4c). The REE chondrite normalized patterns (Fig.4d) show enriched LREE and depletion in HREE with high to moderate $(La/Yb)_N$. The Grt-Bt gneisses show slight negative Eu anomalies (Eu/Eu∗ = 0.7−1.0). The Y-content (20.7−38.16) is high for all samples.

Discussion

The Mauranipur region of the BuC comprises regional metamorphic rocks, ranging from greenschist to upper amphibolite facies. The *P-T* condition in the Mauranipur metapelites has been reported as 5.4 kbar/730°C (Singh and Dwivedi, 2009), and 6.2 kbar/720°C (Singh and Dwivedi, 2015). However, high-grade metamorphism has been recognized from hornblende-biotite-plagioclase bearing gneisses from Sukwan in the Babina region, where *P-T* condition ranges from 6.5–8.5 kbar/630–720°C (Nasipuri *et al*., 2019). Instead, high to ultrahigh pressure amphibolite facies metamorphism is preserved in chlorite-phlogopite-corundum schists with *P-T* condition represented as 11 kbar/630°C and 18 kbar/630°C respectively, from the Babina region (Saha *et al*., 2011). The garnet-bearing BIF from the Mauranipur region reveals a peak temperature ~500°C at 0.1–0.2 GPa, suggesting lower amphibolite facies (Raza *et al*., 2021). In this study, the pseudosection of Grt-Bt gneisses in the NCKFMASHT system has shown peak and retrograde metamorphism. It is clear that the Grt-Bt gneisses were metamorphosed under peak metamorphic conditions in the *P-T* range of 6.35–6.75 kbar and 755–780ºC; here, small grains of Bt, Pl and Qz are embedded into garnet porphyroblast. However, the retrograde metamorphism was recorded sequentially after the peak stage, where a huge mass of biotite was present at the vicinity of garnet grains. This retrograde metamorphic stage was demarcated by 4.80–5.28 kbar and 718–735ºC *P-T* conditions.

The TAS diagram for Grt-Bt gneisses displays contracting protolithic nature varying from diorite, granodiorite and granite

Table 4: Representative major oxides (in wt%), trace elements and REEs (in ppm) compositions of garnet-biotite gneisses.

Oxides	M1	M-1C	M1-A1	M5	M3
SiO_2	60.09	59.29	57.64	77.83	68.56
Al_2O_3	7.46	10.68	16.31	8.48	9.58
FeO	13.91	11.59	10.15	2.61	7.10
TiO_2	1.66	1.45	1.26	0.62	1.03
MnO	0.26	0.24	0.25	0.04	0.14
MgO	8.02	7.89	5.11	0.47	4.18
CaO	3.51	3.10	1.80	2.40	2.75
Na_2O	1.03	1.45	2.02	3.26	2.36
K_2O	0.99	1.13	3.13	2.85	1.99
P_2O_5	0.65	0.39	0.37	0.14	0.27
LOI	2.20	2.52	1.49	1.01	1.42
Total	99.79	99.73	99.54	99.72	99.37
Na_2O+K_2O	2.03	2.58	5.16	6.11	4.35
A/CNK	1.35	1.88	2.34	1.00	1.44
A/NK	3.68	4.14	3.16	1.39	2.76
K_2O/Na_2O	0.96	0.78	1.55	0.87	0.83
Trace elements (ppm)					
V	30.21	34.14	24.53	35.26	21.28
Cr	24.49	19.47	15.79	10.57	24.12
Mn	378.95	2206.10	1667.72	821.34	736.25
Co	5.94	6.92	7.61	5.26	6.70
Ni	4.34	7.21	8.96	6.68	9.21
Cu	7.11	11.48	7.18	14.17	15.25
Rb	205.69	255.64	202.90	258.63	287.31
Sr	155.94	190.72	211.00	74.23	65.28
Nb	21.34	22.83	19.08	19.58	19.09
Mo	2.69	1.08	0.47	1.74	1.66
Cs	7.85	3.74	0.19	16.65	17.55
K	34.52	35.88	29.88	33.20	99.60
Ba	582.38	1505.54	891.41	1537.53	1429.83
Hf	3.64	5.90	0.47	9.04	10.14
Th	9.16	13.61	1.04	18.68	19.77
U	2.94	3.12	0.20	6.01	6.43
La	56.17	51.57	55.36	73.94	69.30
Ce	128.03	102.31	114.05	141.99	138.51
Pr	16.93	11.64	11.94	16.32	15.41
Nd	56.61	45.80	49.51	64.55	61.94
Sm	5.01	9.56	2.93	13.86	13.35
Eu	1.11	2.18	1.15	3.18	3.02
Gd	4.51	9.36	4.21	11.51	11.73
Tb	0.63	1.29	0.69	1.32	1.33
Dy	4.85	7.82	4.77	6.36	6.30
Ho	0.74	1.50	1.02	0.99	1.02
Er	2.21	4.17	3.06	2.41	2.39
Tm	0.32	0.58	0.43	0.31	0.31
Yb	2.12	3.71	2.94	1.87	1.96
Lu	0.33	0.54	0.42	0.29	0.26
Sc	11.69	22.09	52.01	13.23	11.31
Y	20.72	38.16	26.58	26.19	23.61
∑REE	311.99	312.30	331.08	378.29	361.74
$(Ce/Yb)_N$	7.61	7.65	1.33	21.14	19.60
$(Ho/Yb)_N$	1.05	1.21	1.05	1.59	1.56
$(La/Yb)_N$	10.21	9.96	1.31	28.43	25.32
$(La/Sm)_N$	3.89	3.48	1.18	3.44	3.35
$(Gd/Yb)_N$	1.76	2.09	1.19	5.11	4.94
$(La/Lu)_N$	172.79	95.60	130.35	259.38	266.17
$(Lu/Yb)_N$	0.15	0.15	0.14	0.15	0.13
Eu/Eu*	0.72	0.70	1.00	0.77	0.74

(Fig.4a). The granitoids from the BuC also reveal mafic to felsic melt (Rai and Ahmad, 2021). Na and K are highly mobile in nature in the course of metamorphism and hydrothermal alteration; hence, the initial composition of the rock was affected (Deshmukh *et al.*, 2017). The variation of the different major oxides with SiO_2 illustrates a substantial role in the fractionation and crystallization of minerals during the successive evolution of parental magma. The negative anomaly of Nb and Ti for all samples indicates that subduction tectonic setting has been occurred in the BuC. The Grt-Bt gneisses have high SiO_2 and low Cr and Ni concentrations interpreted as protoliths derived from the hydrous thickened lower crust or may be due to crustal contamination with ascending partial melt. The higher $(La/Yb)_N$ and low HREE contents in Grt-Bt gneisses are signatures to the presence of garnet in the source magma during partial melting (Condie, 2005). The Grt-Bt gneisses have small negative Eu anomaly, which indicates the removal of calcic plagioclase from the magma, probably at the initial stage. The Th, La, V, Ce and Sm enrichment is a likely consequence of growth of biotite. Difference in the trace elements and REE abundances (Table 4) and variation in $(La/Lu)_N$ ratio from 95.60 to 266.17, indicates heterogeneous sources and large variation in the degree of partial melting and effect of crustal contamination. The Y vs Nb and (Y+Nb) vs Rb tectonic discrimination diagrams (Fig. 4e-f) show that the protolith of most Grt-Bt gneisses had an affinity towards the volcanic arc granite (VAG), whereas M-1C sample shows within plate granite (WPG) affinity. This study proposes that the Bundelkhand Grt-Bt gneisses are derived mainly from a felsic magma source. This felsic magma is produced by the heat generated during the subduction procedure in the area. However, a detailed study to determine this tectonic evolution would require more geochemical and geochronological data of various rock types, and also the *P-T-t* path will be essential.

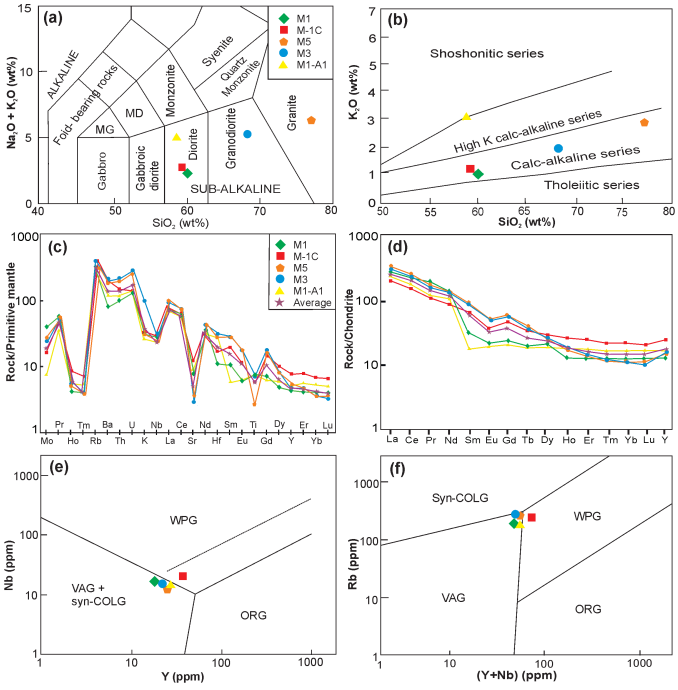

Fig. 4. (a) Total alkali-silica diagram (Le Maitre *et al.,* 1989),(b) SiO_2 vs K_2O plot, (c) Primitive mantle normalized trace element, (d) Chondrite normalized rare earth elements plot of the Grt-Bt gneisses (Sun and McDonough, 1989), (e) Y vs Nb tectonic discrimination diagram and (f) Y+Nb vs Rb tectonic discrimination diagram; Syn-COLG: syn-collisional granite; WPG: within-plate granite; VAG: volcanic-arc granite; ORG: ocean ridge granite (*after* Pearce *et al.,*1984).

Conclusions

The present study has concluded several facts about Grt-Bt gneisses based on petrographic, phase equilibrium modelling and geochemical analysis. The Grt-Bt gneisses have preserved various deformation structures, indicating that they experienced multiple phases of metamorphic events. Phase equilibrium modelling provides *P-T* conditions of the peak metamorphic assemblage at 6.35–6.75 kbar/ 755–780ºC; however, the retrograde metamorphic assemblage is stable at lower *P-T* condition 4.80–5.28 kbar/718–735ºC. The geochemical attributes describe that the protolith is felsic-rich and is developed during the subduction tectonic setting. Simultaneously, the magma was generated during melting of subducted ocean plate in VAG setting of the BuC.

Authors' Contributions

Pratigya Pathak: Field sampling, Conceptualization, Analysis, Investigation, Writing-Original Draft. **Shyam Bihari Dwivedi:** Supervision, Reviewing and Editing. **Ravi Ranjan Kumar:** Conceptualization, Writing-Original Draft.

Acknowledgements

The authors are grateful to the Director, IIT (BHU), for providing the facilities and the first author is thankful to the MHRD Fellowship Scheme for providing financial support.

Conflict of Interest

On behalf of all authors, the corresponding author would like to declare that this manuscript does not have any conflict of interest whatsoever following the Policy of Journal of Geosciences Research.

References

Barik, R., Kaushik, C., Malviya, V.P., Mahapatro, S.N., Shareef, M., Nitnaware, N.V., Sridhar, M., Powar, M.M., Vaidya, P., Khuntia, D.B.K. and Dora, M.L. (2017). Ni-Cu-PGE Mineralisation in Intrusive Mafic Rocks from Ghotitola Area within Amgaon Gneissic Complex, Central India. Jour. Geosci. Res. Spec. v.1, pp. 65-72

Bhowmik, S.K., Wilde, S.A., Bhandari, A., Pal, T., and Pant, N.C. (2012). Growth of the Greater Indian landmass and its assembly in Rodinia: Geochronological evidence from the Central Indian Tectonic Zone. Gondwana Res., v. 22(1), pp. 54–72.

Condie, K.C. (2005). TTGs and adakites: Are they both slab melts? Lithos, v. 80(1), pp. 33–44.

Connolly, J.A.D. (2005). Computation of phase equilibria by linear programming: A tool for geodynamic modeling and its application to subduction zone decarbonation. Earth Planet. Sci. Lett., v. 236, pp. 524-541.

Connolly, J.A.D. (2009). The geodynamic equation of state: what and how.

Geochem. Geophys., v. 10(10), pp. 1–19.

Deshmukh, S.D., Hari, K.R., Diwan, P. and Manu Prasanth, M.P. (2017). Geochemistry and petrogenesis of felsic meta-volcanic rocks of Baghmara Formation, Sonakhan Greenstone Belt, Central India. Jour. Geosci. Res., v. 2(1), pp. 69–74.

Fuhrman, M.L. and Lindsley, D.H. (1988). Ternary-Feldspar Modeling and Thermometry. Am. Mineral., v. 73, pp. 201-215.

Gokarn, S.G., Rao, C.K., Selvaraj, C., Gupta, G. and Singh, B.P. (2013). Crustal Evolution and Tectonics of the Archean Bundelkhand Craton, Central India. Jour. Geol. Soc. India., v. 82, pp. 455-460.

Holland, T. and Powell, R. (2003). Activity-composition relations for phases in petrological calculations: an asymmetric multicomponent formulation. Contrib. Mineral. Petrol., v. 145, pp. 492-501.

Holland, T.J.B. and Powell, R. (2011). An improved and extended internally consistent thermodynamic dataset for phases of petrological interest, involving a new equation of state for solids. Jour. Metamorph. Geol., v. 29, pp. 333-383.

Joshi, K.B., Bhattacharjee, J., Rai, G., Halla, J., Ahamad, T., Kurhila, M., Heilimo, E. and Choudhary, A.K. (2017). The diversification of granitoids and plate tectonic implications at the Archaean Proterozoic boundary in the Bundelkhand Craton, Central India. Geol. Soc. London. Sp. Pub., v. 449(1), pp. 123-157.

Kaur, P., Zeh, A. and Chaudhri, N. (2014). Characterization and U-Pb-Hf isotope record of the 3.55 Ga felsic crust from the Bundelkhand Craton, northern India. Precamb. Res., v. 255, pp. 236–244.

Kaur, P., Zeh, A. and Chaudhri, N. (2021). Archean to Proterozoic (3535–900 Ma) crustal evolution of the central Aravalli Banded Gneissic Complex, NW India: New constraints from zircon U-Pb-Hf isotopes and geochemistry. Precamb. Res., v. 359, pp. 106–179.

Le Maitre, R.W., Bateman, P., Dudek, A.J. and Keller, M.J. (1989). A Classification of Igneous Rocks and Glossary of Terms, Blackwell, Oxford, 193.

Mohan, M.R., Singh, S.P., Santosh, M., Siddiqui, M.A. and Balaram, V. (2012). TTG suite from the Bundelkhand Craton, central India: Geochemistry, petrogenesis and implications for Archean crustal evolution. Jour. Asian Earth Sci., v. 58, pp. 38–50.

Nasipuri, P., Saha, L., Hangqiang, X., Pati, J.K., Satyanaryanan, M. Sarkar, S. Bhandari, A. and Gaur, Y. (2019). Paleoarchean Crustal Evolution of the Bundelkhand Craton, North Central India. *In*: Earth's Oldest Rocks, Elsevier, B.V., pp. 793.

Naqvi, S.M. (2005). Geology and evolution of the Indian plate. Capital Publishing, New Delhi, 450p.

Pandey, R., Chalapathi Rao, N.V., Pandit, D., Sahoo, S., Dhote, P., (2017). Imprints of modal metasomatism in the Post-Deccan subcontinental lithospheric mantle: petrological evidence from an ultramafic xenoliths in an Eocene lamprophyre, NW India. Geol. Soc. London, Special Publication, v. 463(1), pp. 117–136.

Pati, J.K. (2020). Evolution of Bundelkhand Craton. Episodes., v. 43(1), pp. 69-87.

Pearce, J.A., Harris, N.B. and Tindle, A.G. (1984). Trace Element Discrimination Diagrams for the Tectonic Interpretation of Granitic Rocks. J. Petrol., v. 25(4), pp. 956-983.

Pradhan, V.R., Meerta, J.G., Pandit, M.K., Kamenova, G. and Mondal, M.E.A. (2012). Paleomagnetic and geochronological studies of the mafic dyke swarms of Bundelkhand Craton, central India; Implications for the tectonic evolution and paleogeographic reconstructions. Precamb. Res. v. 198–199, pp. 51–76.

Rai, G. and Ahmad, T. (2021). Geochemistry and Petrogenesis of Dioritic-Granodioritic Rocks from Bundelkhand Craton Implications for Precambrian crustal evolution in central Indian Shield. Jour. Geosci. Res., v. 6(1), pp.11–22.

Raza, M.B., Nasipuri, P., Saha, L., Pati, J.K., Alfimova, N.A. and Champati, A.K. (2021). Phase relations and in-situ U-Th-Pbtotal monazite geochronology of Banded Iron Formation, Bundelkhand Craton, North-Central India, and their geodynamic implications. Int. Jour. Earth Sci., pp.1-29.

Saha, L., Pant, N.C., Pati, J.K., Upadhyay, D., Berndt, J., Bhattacharya, A. and Satynarayanan, M. (2011). Neoarchean high-pressure margarite-phengitic muscovite-chlorite corona mantled corundum in quartz-free high-Mg, Al phlogopite-chlorite schists from the Bundelkhand Craton, north Central India. Contrib. Mineral. Petrol., v. 161, pp. 511–530.

Sharma, K.K. and Rahman, A. (2000). The Early Archaean–Paleoproterozoic crustal growth of the Bundelkhand craton, northern Indian shield; In: Crustal Evolution and Metallogeny in the Northwestern Indian Shield, Narosa Publishing House, New Delhi, pp. 51–72

Singh, P.K., Verma, S.K., Singh, V.K., Moreno, J.A., Oliveira, E.P. and Mehta, P. (2019). Geochemistry and petrogenesis of sanukitoids and high-K anatectic granites from the Bundelkhand Craton: Implications for the late-Archean crustal evolution. Jour. Asian Earth Sci., v. 174, pp. 263–282.

Singh, P.K., Verma, S.K., Singh, V.K., Moreno, J.A., Oliveira, E.P., Li, X.H., Malviya, V.P. and Prakash, D. (2021). Geochronology and petrogenesis of the TTG gneisses and granitoids from the Central Bundelkhand granite-greenstone terrane, Bundelkhand Craton, India: Implications for Archean crustal evolution and cratonization. Precamb. Res., v. 359, pp. 106–210.

Singh, S.P. and Dwivedi, S.B. (2009). Garnet–sillimanite–cordierite–quartz bearing assemblages from the early Archean supracrustal rocks of Bundelkhand massif, central India. Curr. Sci., v. 97, pp.103–107.

Singh, S.P. and Dwivedi, S.B. (2015). High grade metamorphism in the Bundelkhand Massif and its implications on Mesoarchean crustal evolution in Central India. Jour. Earth Sys. Sci., v. 124, pp. 197-211.

Singh, S.P., Singh, M.M., Srivastava, G.S. and Basu, A.K. (2007). Crustal evolution in Bundelkhand area, central India. Him. Geol., v. 28(2), pp. 79–101.

Singh, V.K. and Slabunov, A. (2013). The Greenstone belts of the Bundelkhand craton, Central India: new geochronological data and geodynamic setting. *In*: Singh, V.K., and Chandra, R. (*eds*.), International Association for Gondwana Research Conference Series No. 16, 3rd International conference Precambrian Continental Growth and Tectonism, Jhansi, India, pp. 170-171.

Singh, V.K., Slabunov, A., Svetov, S., Rybnikova, Z., Nesterova, N., Gogolev, M., Sibelev, O. and Chaudhary, N. (2018). Occurrence of Archean Iron Bearing Rocks from Babina, Mauranipur and Girar Area of the Bundelkhand Region: As Potential Reserves (SE Siberian Platform). Archeo. Anth., v. 3(3), pp. 108-113.

Sun, S.S. and McDonough, W.F. (1989) Chemical and isotopic systematics of oceanic basalts: Implications for mantle composition and processes. Geol. Soc. London, Sp. Pub., v. 42(1), pp. 313-345.

Tajcmanová, L., Connolly, J.A.D. and Cesare, B. (2009). A thermodynamic model for titanium and ferric iron solution in biotite. Jour. Metamorph. Geol., v. 27, pp. 153–164.

White, R.W., Powell, R., Holland, T.J.B. and Worley, B. (2000). The effect of TiO_2 and $Fe2O_3$ on metapelitic assemblages at greenschist and amphibolite facies conditions: mineral equilibria calculations in the system K_2O-FeO-MgO-Al_2O_3-SiO_2-H_2O-TiO_2-Fe_2O_3. Jour. Metamorph. Geol. v. 18, pp. 497-511.

White, R.W., Powell, R., Holland, T.J.B., Johnson, T.E. and Green, E.C.R. (2014). New mineral activity-composition relations for thermodynamic calculationsinmetapelitic. Jour. Metamorph. Geol. v. 32(3), pp. 261–286.

Whitney, D.L. and Evans, B.W. (2010). Abbreviations for names of rock-forming minerals. Am. Mineral. v. 95, pp. 185-187.

Xiong, F.H., Ma, C.Q., Zhang, J.Y., Liu, B., (2012). The origin of mafic microgranular enclaves and their host granodiorites from East Kunlun, Northern Qinghai-Tibet Plateau: implications for magma mixing during subduction of Paleo-Tethyan lithosphere. Mineral. Petrol. v. 104, pp. 211–224.

Zhai, M. (2014). Multi-stage crustal growth and cratonization of the North China Craton. Geosci. Front., v. 5(4), pp. 457-469.